Field measurements and numerical modelling of wind-driven exchange flows in a tidal inlet system in the Dutch Wadden Sea

van Weerdenburg, Roy ; Pearson, Stuart; van Prooijen, Bram; Laan, Stendert; Elias, Edwin ; Tonnon, Pieter Koen; Wang, Zheng Bing

DOI
10.1016/j.ocecoaman.2021.105941

Publication date
2021

Document Version
Final published version

Published in
Ocean and Coastal Management

Citation (APA)
van Weerdenburg, R., Pearson, S., van Prooijen, B., Laan, S., Elias, E., Tonnon, P. K., & Wang, Z. B. (2021). Field measurements and numerical modelling of wind-driven exchange flows in a tidal inlet system in the Dutch Wadden Sea. *Ocean and Coastal Management*, *215*, 1-12. Article 105941. https://doi.org/10.1016/j.ocecoaman.2021.105941

Ocean and Coastal Management 215 (2021) 105941

Contents lists available at ScienceDirect

Ocean and Coastal Management

journal homepage: www.elsevier.com/locate/ocecoaman

Field measurements and numerical modelling of wind-driven exchange flows in a tidal inlet system in the Dutch Wadden Sea

Roy van Weerdenburg [a,*], Stuart Pearson [b,a,**], Bram van Prooijen [b], Stendert Laan [a], Edwin Elias [a], Pieter Koen Tonnon [a], Zheng Bing Wang [a,b]

[a] Deltares, P.O. Box 177, 2600, MH, Delft, the Netherlands
[b] Faculty of Civil Engineering and Geosciences, Delft University of Technology, P.O. Box 5048, 2600 GA, Delft, the Netherlands

ARTICLE INFO

Keywords:
Wadden sea
Tidal divides
Flow measurements
Exchange flows
Wind-generated currents

ABSTRACT

Multiple tidal inlet systems like the Wadden Sea have long been considered as separated basins, bordered by so-called tidal divides. Recently, it was however shown that fluxes of water and sediment occur over the borders of these basins, especially during wind events. In this paper, the wind-driven fluxes over these borders and the residual flow of water through the main inlet are studied. The study is based on flow measurements at the tidal divides and in the main inlet of the Ameland Inlet system in the Dutch Wadden Sea and on numerical modelling. The measurements were carried out during 40 days in the fall of 2017, including both calm conditions and storm events. Numerical simulations of a full year have been used for upscaling results from the measurements to system scale exchange flows, and to unravel the effects of several mechanisms. The wind-driven variability in exchange flows between back-barrier basins at tidal divides was measured in the field and reproduced by the numerical model. Water level set up increases the water depth and thus the conveyance capacity at tidal divides, such that the exchange flows increase in magnitude. The flow conditions due to wind forcing are similar for both tidal divides of the Ameland Basin. The conveyance capacity and therefore the total volume exchange are however different. This leads to a residual compensation flow through the main inlet, which is directed outward (i.e., in the ebb direction) during winds from the prevailing southwestern wind direction. The net discharge through the main inlet is therefore a consequence of the residual flows over the tidal divides.

1. Introduction

Managers of coastal systems have to weigh the impact of climate change and human interventions on a range of functions (Nicholls and Cazenave, 2010). This includes for example determining the impact of dredging to enable shipping on ecology and tourism, and the impact of climate change on coastal safety and on a subsequent nourishment strategy. To substantiate the choices, a sound understanding of the system is needed, preferably accompanied by a conceptual model (Wang et al., 2018). The understanding of net flows and discharges are at the basis of understanding more complex behaviour of the system, like sediment transport, morphology, or transport of nutrients and larvae. The Dutch Wadden Sea is an example of such a coastal system with a range of functions. Investigating net flows and their effects on the sediment budget of the Wadden Sea is important in view of coastal safety and sea-level rise (e.g. Elias et al., 2012; Wang et al., 2018). For example, sea-level rise and land subsidence due to gas and salt extraction may lead to drowning of intertidal areas if the supply of sediment is limited (e.g. Maan et al., 2019; Van Goor et al., 2003).

Tidal inlets in the Dutch part of the Wadden Sea can be classified as mixed energy wave-dominated environments in the hydrodynamic classification by Davis and Hayes (1984). The exchange of water and sediments through tidal inlets in the Wadden Sea is driven by the combined effects of tidal currents, waves, wind and density effects, as discussed in literature (e.g. Buijsman and Ridderinkhof, 2007; Burchard et al., 2008; Elias et al., 2006). For modelling purposes, topographic highs or tidal divides are often considered as morphological boundaries between basins (Lodder et al., 2019; Van Prooijen and Wang, 2013). An investigation of the sediment budget and bathymetry in the Wadden Sea, however, revealed that exchange of sediment occurs at tidal divides (Elias et al., 2012) and, as a consequence, tidal divides tend to migrate in time (Wang et al., 2013).

* Corresponding author.
** Corresponding author. Faculty of Civil Engineering and Geosciences, Delft University of Technology, P.O. Box 5048, 2600 GA, Delft, the Netherlands.
E-mail address: Roy.vanWeerdenburg@Deltares.nl (R. van Weerdenburg).

https://doi.org/10.1016/j.ocecoaman.2021.105941
Received 26 February 2021; Received in revised form 21 September 2021; Accepted 8 October 2021
Available online 23 October 2021

Differences in water-level amplitude between inlets may cause a residual circulation between tidal basins (Liu and Aubrey, 1993; Van de Kreeke and Cotter, 1974), which is the case in the western Dutch Wadden Sea (Ridderinkhof, 1988a, 1988b). Whereas tidal divides in the western Dutch Wadden Sea are still relatively deep, such that exchange flows are less limited by the flow depth, recent modelling studies (Duran-Matute et al., 2014, 2016; Herrling and Winter 2015; Sassi et al., 2015) also suggest exchange at shallower tidal divides in the Wadden Sea. Duran-Matute et al. (2016) conclude that during certain (i.e., strong) wind conditions, the tidal divide of the island Terschelling in the Dutch Wadden Sea can no longer be considered as a closed barrier between the two adjacent basins. Residual exchange flows across this tidal divide become significant because the dominant wind direction is also the preferential direction for exchange flows (Duran-Matute et al., 2016). The Dutch Wadden Sea may then be considered as a multiple tidal inlet system or single contiguous estuary. Wind forcing on multi-inlet systems can lead to circulations with residual in- and outflows through each of the inlets, depending on the wind direction and differences in bed elevation (Li, 2013).

Although the exchange between adjacent basins (i.e., two basins separated by a tidal divide and connected to different tidal inlets) has been investigated in modelling studies, there have been few field measurements to support the findings. Vinther et al. (2004) were probably the first to publish about flow and sediment transport measurements at a tidal divide in the Wadden Sea, although at a tidal divide separating two sub-basins (i.e., connected to the same tidal inlet). It was found that current velocities by the asymmetrical tide were significantly strengthened when the wind was blowing in the direction of the flood current. A crucial role of wind was also found in the field measurements of Colosimo et al. (2020). They showed that the impact of wind on flow is non-linearly depending on the background tidal current: the weaker the tidal current, the stronger the effect of wind. This suggests a significant impact of wind at tidal divides, where tidal currents are generally small. Systematic measurements at tidal divides with the explicit goal of quantifying inter-basin flow are however lacking. Such measurements would not only provide insight into the exchange flows at the measurement locations, but are also essential for the calibration and validation of process-based numerical models.

The aim of this study is to (1) understand and quantify the net exchange flows of water at tidal divides of the Ameland Inlet system, and (2) explain how these are related to residual flows through Ameland Inlet. We aim to answer the question whether the residual discharge through the Ameland Inlet is the cause or a consequence of the net discharge over the tidal divides. The study area, the collection and processing of field data, and the numerical modelling approach are discussed in Section 2. Flow measurements obtained in the tidal inlet and at the two tidal divides during a field campaign in September 2017 are presented (Section 3.1). The flow measurements are used to calibrate and validate a numerical model of the Dutch Wadden Sea. The model is used for the upscaling of point measurements to system scale exchange flows and to unravel the effects of several forcing mechanisms on exchange flows at the tidal divides and in the inlet (Section 3.2). The discussion of results (Section 4) includes a synthesis, the representativeness of conditions during the measurement campaign, and implications. Conclusions are given in Section 5.

2. Materials and methods

2.1. Study area

The Wadden Sea is a multiple tidal inlet system that spans a distance of nearly 500 km between the northwestern part of the Netherlands to the North Sea coast of Denmark. It is the world's largest coherent system of intertidal flats and was declared a World Heritage site by UNESCO in 2009. The Dutch part of the Wadden Sea (the West Frisian Islands) extends from Texel Inlet in the west to the Ems-Dollard estuary in the east (Fig. 1). The Dutch Wadden Sea is separated from Lake IJssel (containing fresh water) by a closure dam (*Afsluitdijk*), which was constructed in the early 20th century. Tidal inlets separate five inhabited islands in the Dutch Wadden Sea (Fig. 1).

Ameland Inlet is centrally located in the Dutch Wadden Sea, between the barrier islands Terschelling and Ameland (Fig. 1). The back-barrier basin of Ameland Inlet is bounded by the mainland coast and the Terschelling and Ameland tidal divides (i.e., between Terschelling and the mainland coast and between Ameland and the mainland coast, respectively). The back-barrier basin has a length of roughly 30 km and covers an area of approximately 270 km^2. Around 60% of the basin consists of intertidal shoals. The back-barrier basin becomes smaller towards the east, due to the underlying Pleistocene morphology (Van der Spek, 1995). The main ebb-channel in the tidal inlet is located along the west coast of Ameland (Fig. 2). The maximum water depth in this channel exceeds 25 m. In the basin, the channels bifurcate into multiple

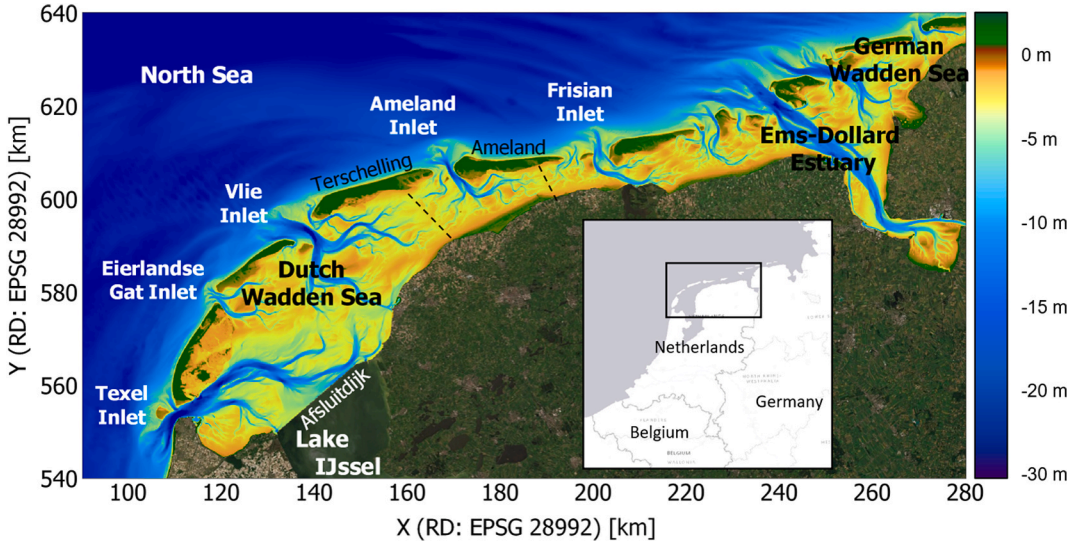

Fig. 1. Bathymetry in the Dutch Wadden Sea relative to local reference height NAP (equivalent to MSL; bathymetry source: Rijkswaterstaat Vaklodingen), with indicated the islands and tidal inlets in the Dutch Wadden Sea. This study focusses on Ameland Inlet system. The approximate locations of the tidal divides of Terschelling and Ameland are indicated by dashed lines.

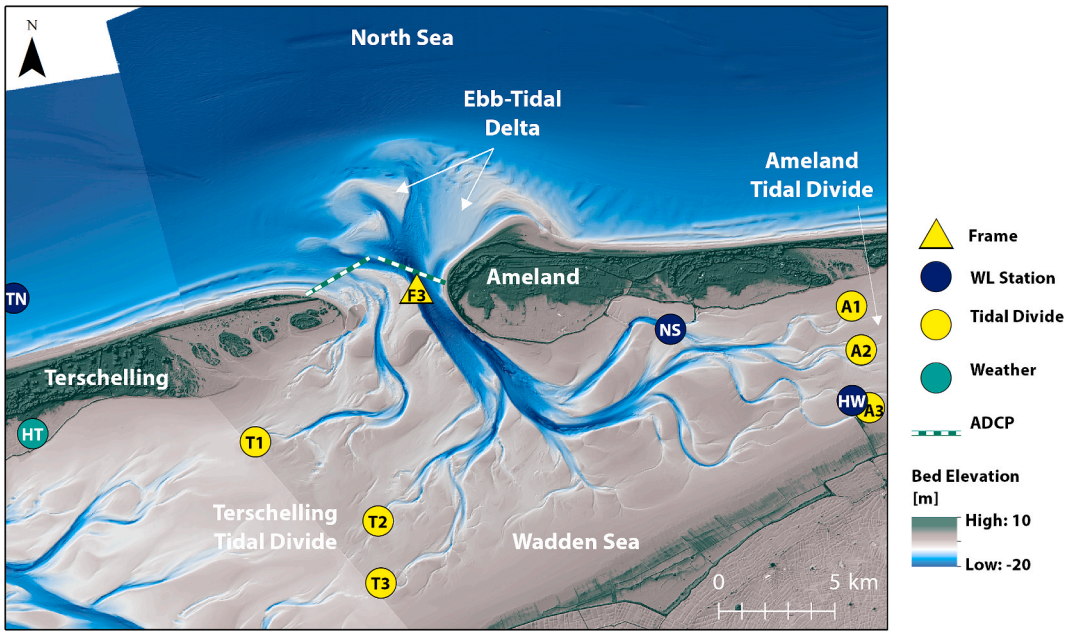

Fig. 2. Locations where hydrodynamic and atmospheric measurements were carried out during the field campaign in the fall of 2017. Water level stations: Terschelling Noordzee (TN); Nes (NS); Holwerd (HW). Weather station: Hoorn Terschelling (HT). Elevation and bathymetry source: Actuele Hoogtebestand Nederland (AHN) and Vaklodingen, Rijkswaterstaat.

smaller channels towards the tidal divides, separating intertidal areas (Fig. 2).

2.2. Field measurements

In the fall of 2017, a 40-day field campaign (August 29 – October 9) was carried out in and around Ameland Inlet (Van Prooijen et al., 2020). Among other measurement locations, a measurement frame was deployed at the westerly margin of the main inlet channel (F3 in Fig. 2). The mean local water depth at this location was 16.3 m during the field campaign. The frame was equipped with multiple instruments (Van Prooijen et al., 2020). For this paper, flow velocities that were measured by an upward-looking ADCP and a pressure record of an Aquadopp HR Profiler are used. The ADCP measured three-dimensional flow velocities over the full water column at a resolution of 1.25 Hz. The pressure sensor measured at a temporal resolution of 4 Hz. About halfway through the measurement campaign (September 18), the frame was retrieved to the water surface for inspection and maintenance. Afterwards, it was relocated at approximately the original location for the second part of the measurement campaign. The height of bins in which flow velocities were measured by the ADCP was 1.0 m in the first part and 0.8 m in the second part of the field campaign.

Three Aquadopp HR profilers were installed for a full month at each of the tidal divides of Terschelling and Ameland (Fig. 2). The instruments were located approximately at the end of channels in the back-barrier basin. The Aquadopp HR profilers were pushed vertically into the sand, such that an upward directed acoustic beam measured flow velocities every minute in 45 bins of 0.1 m. One of the instruments

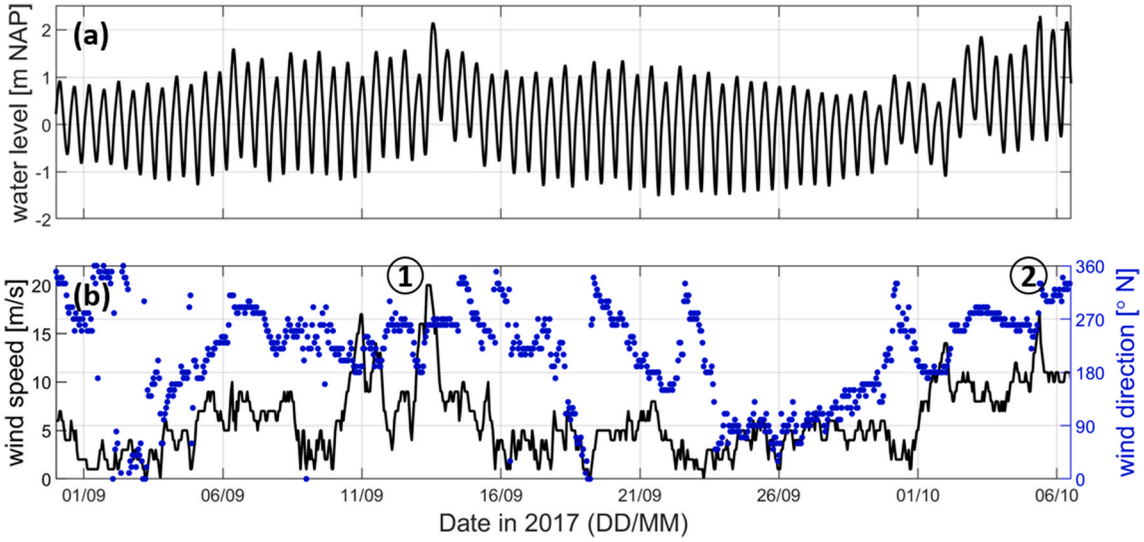

Fig. 3. Time series [a] of measured water levels at Nes and [b] of the wind speed (black line) and direction (blue dots) at Hoorn, Terschelling, during the field campaign. Storms Sebastian [1] and Xavier [2] are indicated in the time series of wind conditions. (For interpretation of the references to colour in this figure legend, the reader is referred to the Web version of this article.)

(T2) stopped measuring flow velocities halfway through the field campaign, as it became buried with sediment.

Discharge measurements were carried out for three periods of 13 h at two transects in the tidal inlet (Fig. 2). The discharge measurements extend 13 h to cover a full tidal cycle. Every 20 min, two vessels equipped with a downward-looking ADCP sailed along the same transects to measure vertical velocity profiles. The combined measurements of the two vessels provides estimates of the total discharge through the inlet, which are used for validation of the numerical model.

Permanent water level stations are located at Nes (NS), at Holwerd (HW) and at Terschelling Noordzee (TN in Fig. 2). The water level variation measured at Nes (Fig. 3a) indicates periods of significant set-up in the back-barrier basin during mid-September and in the beginning of October. Wind conditions (i.e., wind speed and wind direction) and air pressure fluctuations are measured at a permanent meteorological station of KNMI (Royal Netherlands Meteorological Institute) at Hoorn, Terschelling (HT in Fig. 2; Fig. 3b). Wind around Ameland Inlet is predominantly from the west-southwest. Strong winds (>16 m/s) were observed more frequently during the measurement campaign (2.1% of time) than on average in 2017 (0.6% of time). Wind speeds reached up to 20 m/s during Storm Sebastian (peak at September 13, [1] in Fig. 3), and up to 17 m/s during Storm Xavier (peak at October 5, [2] in Fig. 3). The period between the two windstorms was fairly calm, with maximum wind speeds around 5–6 m/s.

2.3. Data processing

Recorded pressure signals are corrected for atmospheric pressure fluctuations to obtain water pressure. The water depth above the pressure sensor in the inlet (Frame 3) was determined according to linear wave theory. At the tidal divides, pressure was measured every minute. Since this temporal resolution is too low to capture surface waves, time series of the water depth are determined by assuming hydrostatic pressure conditions.

The reference height of ADCP velocity measurements in the nth bin from the seabed is defined as:

$$z_u(n) = z_{instrument} + z_{mid,bin1} + (n-1)\,dz \tag{1}$$

where $z_{instrument}$ is the height of the instrument above the seabed, $z_{mid,bin1}$ is the distance from the top of the instrument to the center of the first bin (i.e., including the blanking distance of the instrument), n is the bin number, and dz is the bin size. Measured velocities are converted from XYZ velocities relative to the orientation of the instrument into East-North-Up (ENU) velocities using the heading, pitch and roll (HPR) of instruments.

Velocity records are filtered based on the correlation with the signal-to-noise ratio (Elgar et al., 2005) and despiked using a 3D phase space method (Goring and Nikora, 2002; Mori et al., 2007). A detailed description of the processing of data from the field campaign is included in the data report (Van der Werf et al., 2019).

Specific discharges (i.e., per unit width) are determined from the ADCP velocity data as:

$$\boldsymbol{q}(t) = \sum_{i=1}^{N} \boldsymbol{u}_i(t,\, z_i)\,dz \tag{2}$$

where discharge and velocity vectors $\boldsymbol{q}$ and $\boldsymbol{u}$ have an east and a north component, N is the number of bins that are completely below the water surface, and dz is the bin size. In case velocity measurements do not reach the water level at a certain time step, near-surface velocities are assumed equal to the mean of the velocities in the upper five bins with available data. Near-bottom velocities (i.e., below the first bin of the velocity profile from the bottom) are estimated as the mean of zero and the velocity value in the first bin from the bottom. The accuracy by which the specific discharge is determined depends on the accuracy of measurements of the water depth and the velocity profile. The accuracy reduces for lower water depths, as the number of velocity bins below the water surface reduces (i.e., less data points in vertical direction).

2.4. Numerical modelling: set-up, calibration, validation and scenarios

2.4.1. Model set-up

A depth-averaged hydrodynamic model of the Dutch Wadden Sea has been set-up in Delft3D Flexible Mesh. This numerical model simulates tides, surge and the effects of wind and atmospheric pressure fluctuations. Ameland Inlet is centrally located in the model domain (Fig. 4). The grid resolution increases in four refinement steps from 4 km in the southwestern corner towards characteristic grid cell sizes of around 30–50 m in Ameland Basin (Fig. 4b). The model bathymetry is based on a composite of bathymetric surveys from 2014 to 2017, with 2017 surveys in Ameland Inlet and Basin (Rijkswaterstaat Vaklodingen on a 20 m × 20 m grid, obtained by single-beam echo sounders in 3-year and 6-year intervals for ebb-tidal deltas and basins, respectively). The hydrodynamic model is forced by water level boundaries and meteorological conditions. Time series of the water level variations due to tides and surge are prescribed at the seaward boundaries. The water level boundary conditions are derived from the DCSMv6-ZUNOv4 model with Kalman filtering of the northwest European shelf (Zijl et al., 2013). The meteorological forcing (i.e., wind vector and atmospheric pressure) is based on the ERA5 atmospheric reanalysis (Hersbach et al., 2020) by the European Centre for Medium-Range Weather Forecasts (ECMWF). This model provides hourly data on a 30 km resolution grid. The wind speed contributes to a shear stress in the momentum equations using the Charnock (1955) wind drag formulation. The Charnock coefficient is space and time varying, following the ERA5 data.

2.4.2. Model calibration

The model was calibrated by adjusting the bottom roughness such that measured water levels and tidal propagation at permanent water level stations in the model domain were reproduced accurately (Fig. 5). Using a uniform Manning roughness of 0.022 s/m$^{1/3}$ leads to the best reproduction of observed water levels. The Manning roughness was locally increased to 0.028 s/m$^{1/3}$ in the basins of Texel Inlet and Eierlandse Gat Inlet. This was needed to dampen the reflection of the tidal wave in these basins, which led to an increased amplitude in the tidal inlets and basins in simulations with a lower roughness. After calibration, the model accurately reproduces water level variations by tides and surge (Fig. 5). Based on an analysis of modelled water levels in 2017 at 15 stations in and around the Wadden Sea, the average absolute bias is 3.1 cm. The average standard deviation of the error signal of the total water level reproduction (i.e. variations due to tide and surge) is 7.1 cm (Fig. 5). The average standard deviation of reproducing tidal water level variations is 5.6 cm.

2.4.3. Model validation

The numerical model was validated with measured flow velocities and the discharge measurements taken in Ameland Inlet. The amplitude and the phasing of computed flows show good correspondence with measurements, as illustrated by the reproduction of discharge measurements in Fig. 6. This indicates that spring-neap variations are captured well in the model, since the tidal range is different for each of the three periods (i.e., neap tide at September 1, spring tide at September 19 and between neap and spring tide at September 5). Also, the meteorological conditions were different for each of the three periods (i.e., calm wind from the northwest at September 1 and at September 19 and moderate wind from the southwest at September 5). Minor differences between the measured and computed discharges occur during maximum flood discharge (i.e., larger maximum flood discharge in model results) and during high water slack at September 1 and September 5 (i.e., computed discharge ahead of measured discharge). The difference in cumulative discharge through the inlet

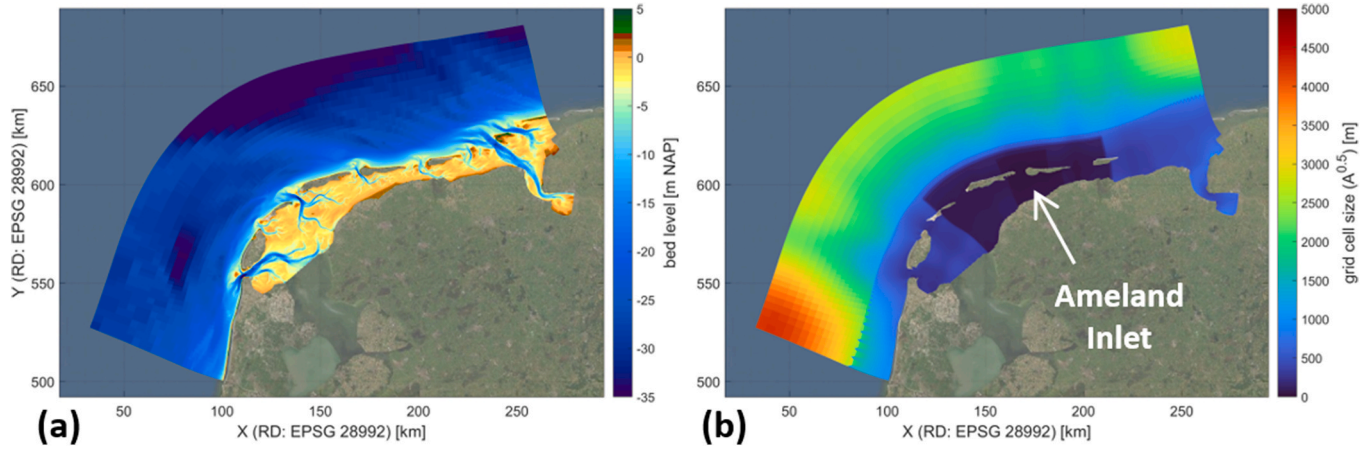

Fig. 4. Domain and schematization of the Delft3D Flexible Mesh model of the Dutch Wadden Sea: [a] bathymetry relative to local reference height NAP and [b] grid resolution, with multiple grid refinements towards Ameland Inlet.

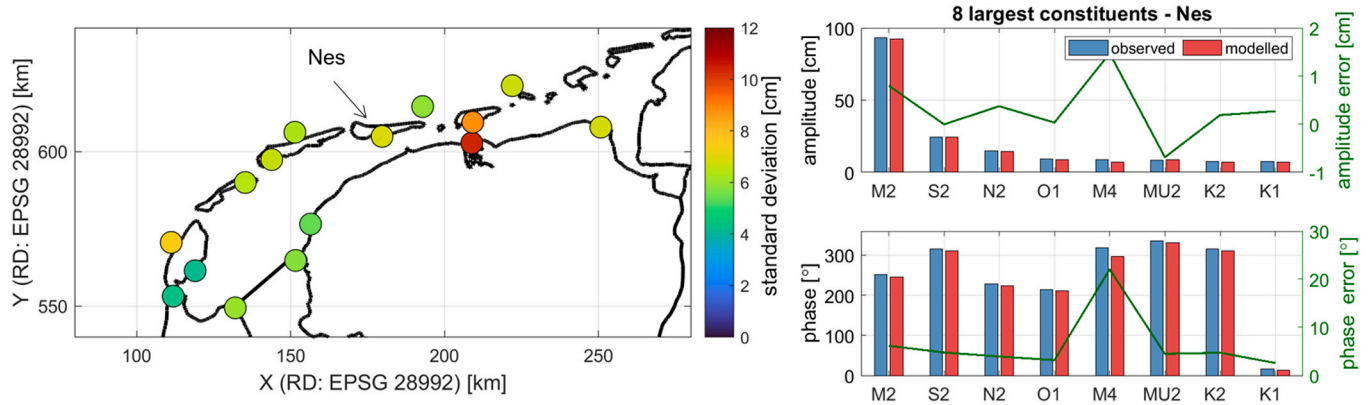

Fig. 5. Reproduction of observed water levels in 2017 by the numerical model: [left] standard deviation of the reproduction of total water level variations at 15 water level stations in and around the Wadden Sea and [right] comparison between observed and modelled tidal constituents (amplitude and phase) at Nes.

between model and measurements is 2–6%, which is considered to be within the range of accuracy of the measurements. The cumulative discharges in model results are larger than measured cumulative discharges during ebb and flood for all three tidal periods.

The residual (i.e., tide-averaged) flow through the tidal inlet during the 13-h measurement periods is only a few percent of the integrated flood and ebb volumes. It is of the same order of magnitude as the range of accuracy of the discharge measurements and of the reproduction by the numerical model (Fig. 6). The discharge measurements are therefore of limited value to investigate the accuracy of the numerical model to quantify residual flows. However, the residual flow through the inlet depends on the exchange between basins at the tidal divides. The reproduction of these exchange flows supports that the numerical model can be used to investigate residual flows within acceptable accuracy limits. Measured and modelled flow variations at the tidal divides are included in Section 3.

2.4.4. Model scenarios

To investigate the importance of the various processes, four model simulations were executed for the year 2017. The first simulation includes all boundary conditions that were introduced (i.e., tide, surge and meteorological forcing). In the second simulation, surge variations were removed from the model boundaries. The third simulation does include surge variations, but the meteorological forcing was removed. The fourth simulation does only include tidal variations. Although surge variations and meteorological forcing are in reality often coupled, we aim to unravel the effects of the two forcing mechanisms. These are therefore switched on and off separately in different model scenarios. Model results of water levels and discharges through cross-sections in Ameland Inlet and at the Terschelling and Ameland tidal divides are included in this paper.

3. Results

3.1. Measured flows in the tidal inlet and at tidal divides

The main tidal constituent (i.e., M2) has an amplitude of 0.86 m at the observation point in the tidal inlet. Tidal currents are aligned with the orientation of the main channel, such that the velocity component to the north is multiple times larger than to the east. Measured flow velocities reach up to 1.5 m/s during spring tide (Fig. 7a). At this location in the inlet, peak flow velocities during ebb are usually larger than during flood. The residual discharge per tidal period is usually in the ebb direction, as indicated by the black dots in Fig. 7b. This means there is a residual outflow from the basin at this location on the west side of the inlet. The mean magnitude of the residual discharge is 2.1 m^2/s (i.e., discharge per unit width) and the variability between tidal periods is quantified by a standard deviation of 1.05 m^2/s. During the maximum residual outflow on September 13 ([1] in Fig. 7b), the measured residual discharge towards the north was up to 3.2 times the average residual discharge during the field campaign.

Measurements at the tidal divides yield time series of the local water depth, flow velocities and discharges (i.e., after integration over depth). At these tidal divides, the water depth generally varies between 0 and 2

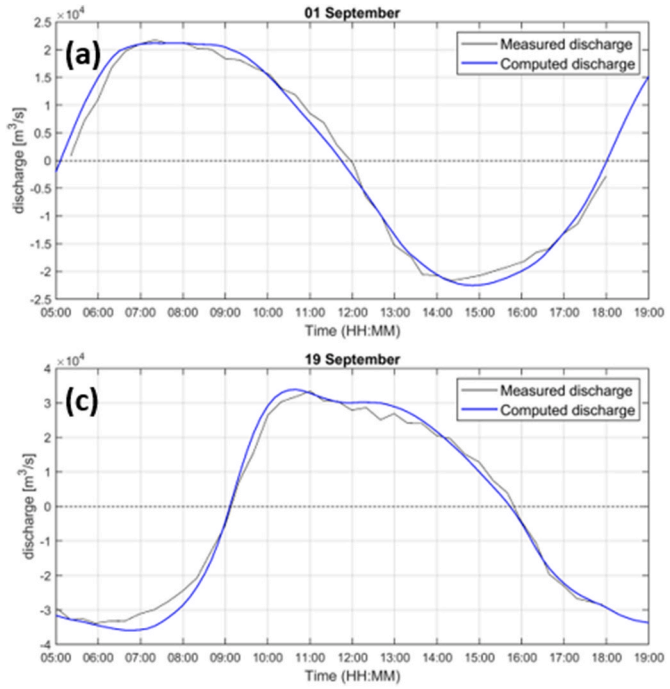

		Measured	Computed
01/09	Qflood	350*10⁶ m³	359*10⁶ m³ (+3%)
	Qebb	331*10⁶ m³	336*10⁶ m³ (+2%)
05/09	Qflood	467*10⁶ m³	491*10⁶ m³ (+5%)
	Qebb	462*10⁶ m³	479*10⁶ m³ (+4%)
19/09	Qflood	525*10⁶ m³	555*10⁶ m³ (+6%)
	Qebb	532*10⁶ m³	566*10⁶ m³ (+6%)

Fig. 6. Comparison between measured and computed discharge through Ameland Inlet for three 13-h periods in September 2017. The table lists integrated volumes in flood (negative) and ebb (positive) direction.

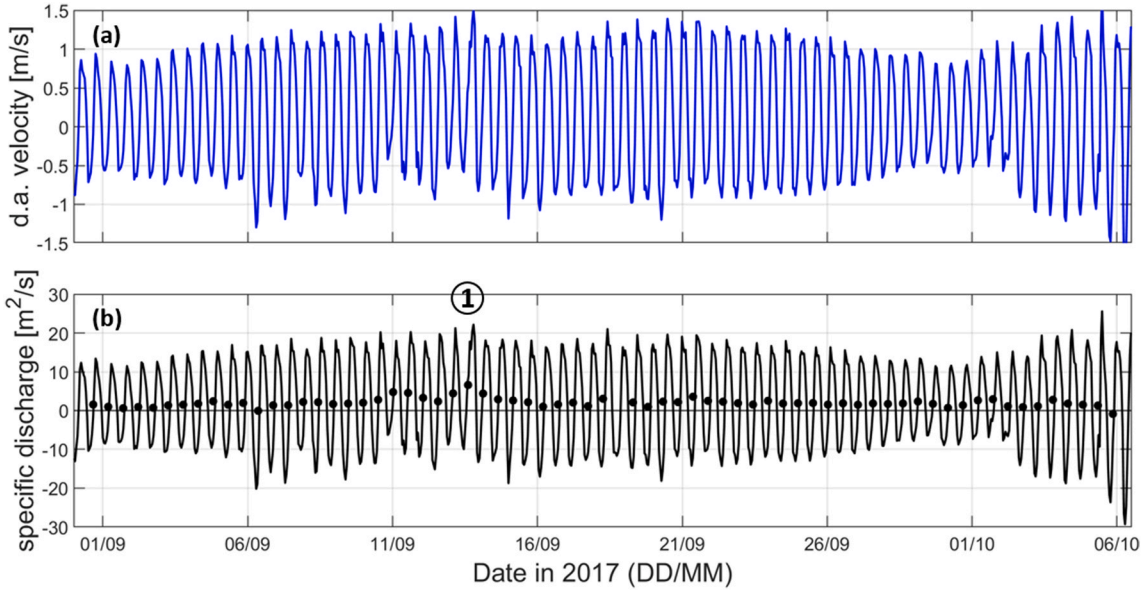

Fig. 7. Time series of [a] the measured depth-averaged flow velocities in the principal flow direction and [b] specific discharge at the measurement frame in the tidal inlet (Frame 3; depth-integrated) during the field campaign. Outflow (i.e., ebb) is considered in the positive direction. Black dots indicate the average discharge per M2 tidal period. [1] indicates the maximum residual outflow on September 13.

m (Fig. 8), although water level set-up during the field campaign caused water depths during high water to exceed 3 m. The low water levels usually did not exceed the blanking distance of the instruments (0.15 m), resulting in gaps in the time series of measured flow velocities and discharges around low water (Fig. 8). The time series of depth-integrated discharges show large differences between tidal periods in both the magnitude and the direction of the (residual) flow. Most striking is the large peak discharge towards the east, with flow velocities exceeding 1 m/s, during the windstorm on September 13. The time series suggest a positive correlation between the local water depth and the observed discharge, which will be investigated further using the numerical modelling results.

The tide-averaged flows that are computed from instantaneous flow measurements depend on the definition of a tidal period, for which multiple possibilities exist (Duran-Matute and Gerkema, 2015). Here, a tidal period in measurements is defined as an M2 tidal period, starting at low water. This definition is chosen because the drying of tidal divides causes gaps in timeseries around low water. These gaps are naturally adopted as separation between successive tidal periods. For consistency, this definition is also applied for flow measurements in the inlet.

The residual discharge per tidal period at Frame 3 in the inlet is generally directed out of the tidal basin, as the measurement frame lies

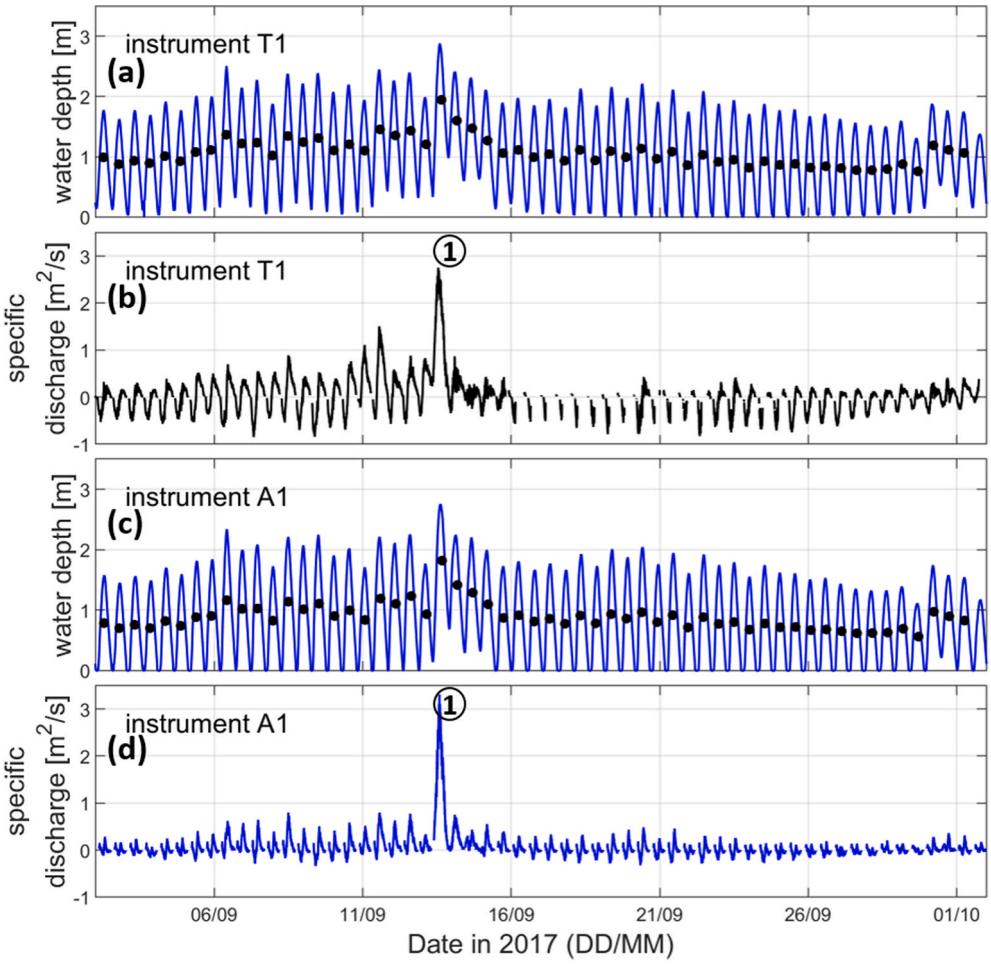

Fig. 8. Time series of the local water depth and specific discharge in the principal flow direction at measurement locations [a, b] at the Terschelling tidal divide (T1) and [c, d] at the Ameland tidal divide (A1). Flow towards the east is considered in the positive direction. Black dots indicate tide-averaged water levels. [1] indicates the large eastward flow on September 13.

in an ebb-dominant part of the channel. To a large extent, the variability in the residual discharge can be explained by the wind forcing (Fig. 9). Residual outflows are above average in magnitude during moderate and strong winds from the west and southwest. When tide-averaged wind speeds reached 15.8 m/s from the west (262°N) during the peak of the first windstorm on September 13, the largest residual discharge was observed (6.7 m^2/s; tidal period indicated as the longest black arrow in Fig. 9). Although wind conditions decreased to moderate wind speeds after the peak of the storm, the observed residual discharge remained relatively high for two more tidal periods (i.e., 4.3 and 2.9 m^2/s). The two successive tidal periods, in which w_{sp} = 8.3 m/s (263°N) and w_{sp} = 7.5 m/s (316°N) respectively, are indicated in black in Fig. 9. During these tidal periods after the peak of the storm, the water level set-up in the tidal basin decreased, causing a time lag effect between the wind forcing and the residual flow in the inlet. The residual discharge was directed towards the tidal basin for only one tidal period in the record, when the tide-averaged wind speed was 10.6 m/s from the northwest (306°N) during the second windstorm in the field campaign.

As illustrated for the Terschelling tidal divide by a numerical modelling study by Duran-Matute et al. (2016), the variability in the residual exchange over the tidal divides can to a large extent be explained by the wind forcing. This is also found in the field observations at the tidal divides of Terschelling and Ameland, as illustrated for one of the three measurement locations at each of the tidal divides in Fig. 10. During calm wind conditions, residual discharges are generally small. The direction of the residual discharges during calm wind conditions varies between the measurement locations, probably because of local effects (e.g., position of the instrument relative to channels and shoals). During moderate to strong winds (>~5 m/s) from the west and southwest, residual discharges at both tidal divides are eastward directed and the residual discharge increases in magnitude with increasing wind speeds (Fig. 10). The residual discharges per tidal period suggest that exchange at the Terschelling tidal divide is more sensitive to winds from the west-southwest, whereas exchange at the Ameland tidal divide is more sensitive to winds from the west-northwest. This could be explained by the orientation of the tidal divides in the Wadden Sea; further towards the east, the orientation of the Dutch Wadden Sea changes from southwest-northeast to west-east (Fig. 1).

3.2. *Upscaling using model results*

Model results of the 1-year simulation were used to determine the residual discharge per tidal period over the tidal divides of Terschelling and Ameland. The variability of the residual discharges with the tide-averaged wind conditions are in agreement with the field observations (Fig. 11). During strong winds from the west to southwest (~15 m/s), the residual discharge integrated over the Terschelling tidal divide exceeds the average tidal prism of Ameland Inlet in model results for 2017 (i.e., up to 1.25 times the average tidal prism of 450 million m^3).

The residual discharge per tidal period at the Ameland tidal divide is generally several times smaller than at the Terschelling tidal divide.

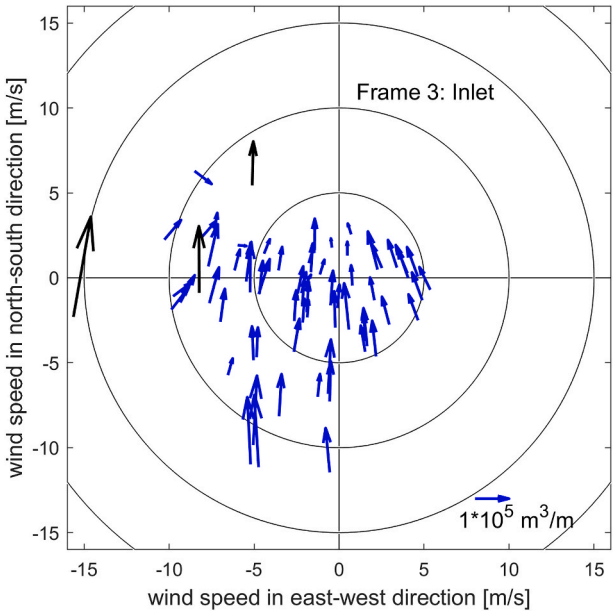

Fig. 9. Residual discharge per tidal period in relation to the tide-averaged wind conditions at a measurement frame (Frame 3) in the tidal inlet. The arrows indicate the magnitude and direction of the residual discharge per tidal period. The position of an arrow's tail in the figure indicates the wind conditions. Black arrows relate to Storm Sebastian on September 13.

There is a strong correlation between the residual discharges per tidal period at both tidal divides (linear correlation coefficient $\rho = 0.91$). A linear fit through the points in Fig. 11c has a slope of 0.31. This suggests that if the residual discharge at the Terschelling tidal divide increases 1 m^3/s, an increase of 0.31 m^3/s could be expected at the Ameland tidal divide. This ratio can be explained by the conveyance area at the two tidal divides (Fig. 12). The Ameland tidal divide is smaller than the Terschelling tidal divide, such that the conveyance capacity at mean water level is approximately 0.36 times smaller.

When comparing the variability with wind conditions at the two tidal divides, the peak in residual discharge has shifted slightly from west to southwest for Terschelling to west for Ameland. A similar shift was already suggested when discussing the field measurements in Section 3.1 of this paper. It could be explained by the shape of the Dutch Wadden Sea, and hence the orientation of the tidal divides. Winds from the west to southwest are directed perpendicular to the orientation of the Terschelling tidal divide, whereas winds from the west are directed perpendicular to the orientation of the Ameland tidal divide. This leads to a different ratio between the residual discharges at the two tidal divides for different wind directions (i.e., as can be seen in the distribution of colours in Fig. 11c, at different sides of the linear fit).

The difference in residual flow over the two tidal divides leads to a residual outflow through Ameland Inlet (Fig. 13). The computed cumulative discharge over Terschelling tidal divide into Ameland Basin in 2017 is $2.8*10^{10}$ m^3. Around 53% of this amount (i.e., $1.5*10^{10}$ m^3) flows out of the basin via the Ameland tidal divide. 47% of the inflow at Terschelling tidal divide (i.e., $1.3*10^{10}$ m^3) flows out via Ameland Inlet. The mean residual outflow due to the exchange at tidal divides in 2017 is 4% of the mean tidal prism of Ameland Inlet.

Removing surge variations from the model boundaries reduces the magnitude of cumulative exchange flows with 17–25%, while temporal variations remain similar (Fig. 13). This indicates that large-scale surge levels do not generate but facilitate significant residual flows at the tidal divides. The water level gradient that generates the residual flow at the tidal divides is primarily generated locally (i.e., within the model domain), as illustrated in Fig. 14 for the moment of maximum throughflow in September 2017. The surge levels in model simulations with and without surge variations at the model boundaries are here determined as the water level relative to the model simulation with only tidal forcing. Locally generated surge levels increase in the direction of the wind in the different basins (i.e., from west to east in Fig. 14). This leads to a relatively strong water level gradient in opposite direction at the tidal divides, which generates a flow towards the east. North Sea surge (i.e., imposed at the model boundaries) increases the water level, without imposing significant additional water level gradients at the spatial scale of the tidal basin.

The exchange flows in a simulation without wind forcing (Fig. 13) are similar to flows during calm wind conditions (Fig. 12). A relatively small residual flow over the Terschelling tidal divide in eastward direction remains, with hardly any variation throughout the year. Without wind forcing, the residual flow over the Ameland tidal divide is larger than the residual flow over the Terschelling tidal divide. Hence the residual flow through Ameland Inlet is directed inward without wind forcing, whereas it is directed outward when wind forcing is included.

4. Discussion

4.1. Synthesis

At the Terschelling and Ameland tidal divides, the variability in

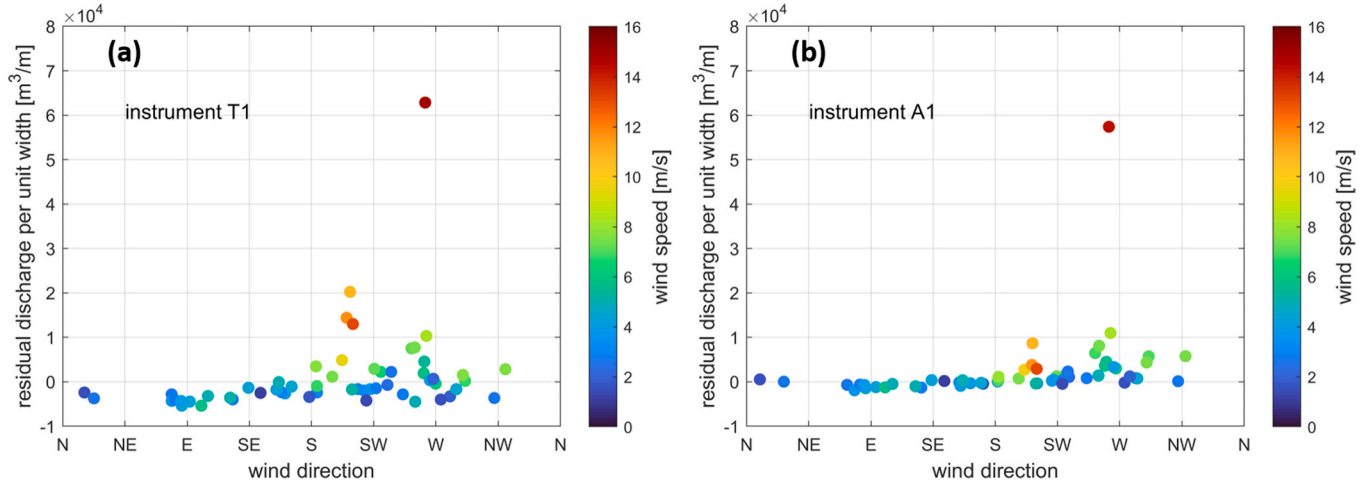

Fig. 10. Residual discharge per M2 tidal period in relation to the tide-averaged wind conditions at measurement locations at the tidal divides of [a] Terschelling (T1) and [b] Ameland (A1).

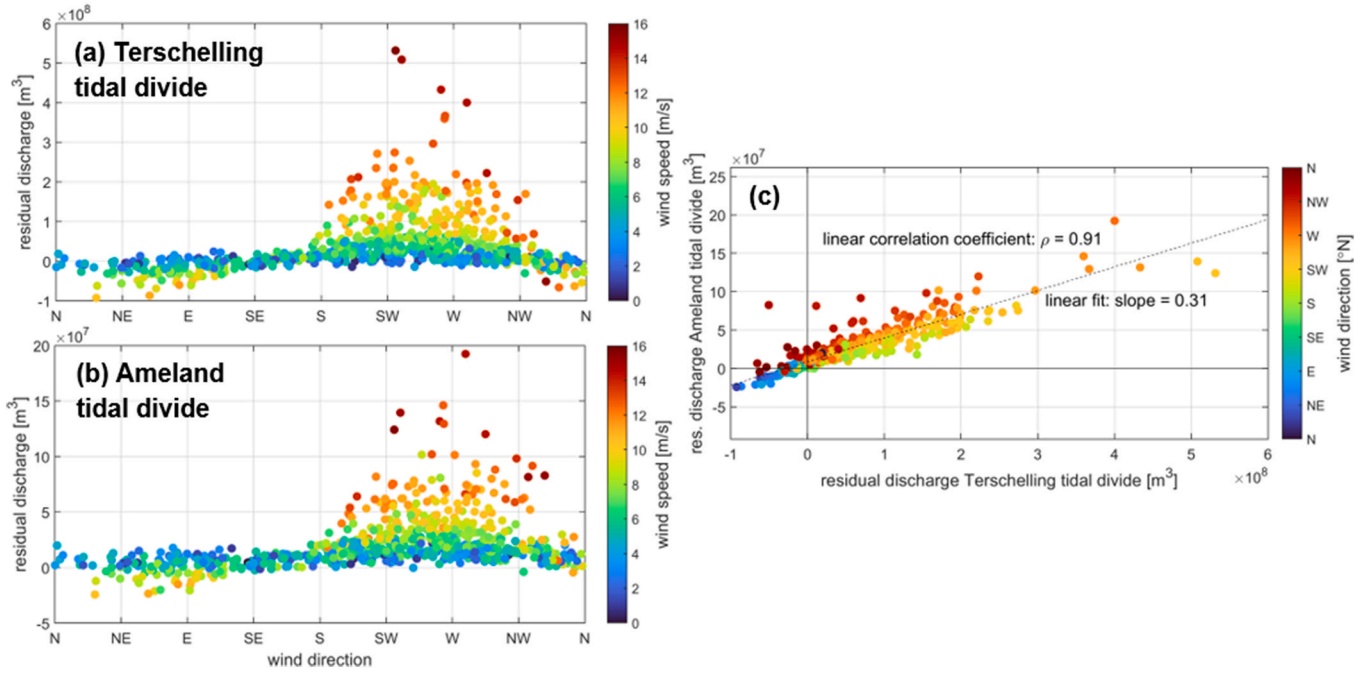

Fig. 11. Residual discharge per tidal period in 2017 in relation to tide-averaged wind conditions for [a] Terschelling tidal divide and [b] Ameland tidal divide and [c] the relation between the residual discharges over the two tidal divides. Eastward flow is considered in the positive direction.

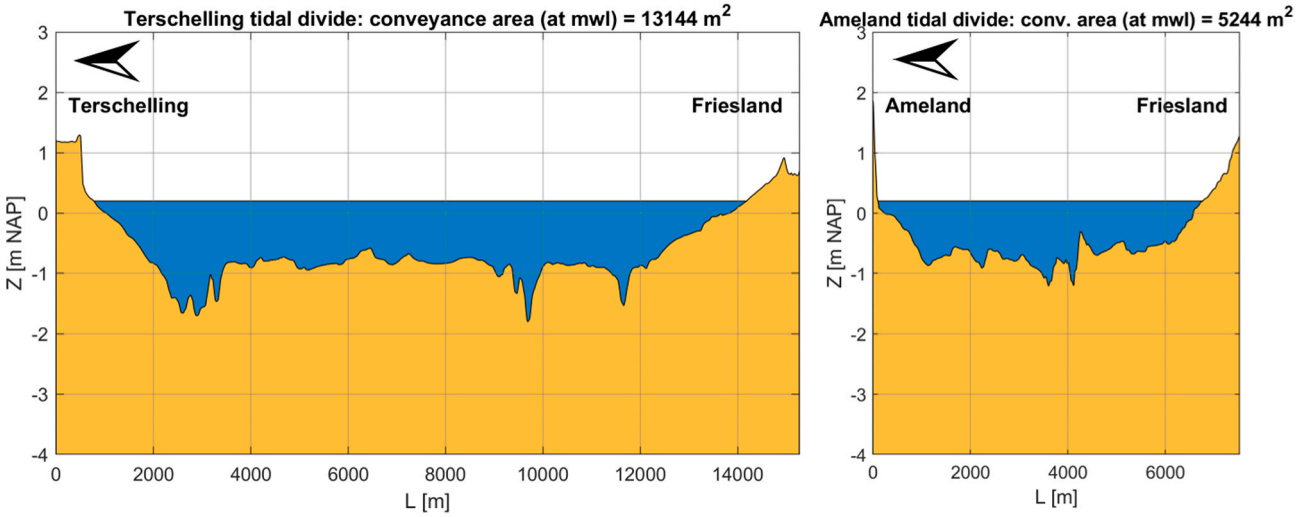

Fig. 12. Bathymetry in a cross-section at the tidal divides of [left] Terschelling and [right] Ameland. The illustrated water surface is at mean water level.

residual flows is primarily generated by local wind forcing. Surge may be separated into a locally generated surge level and a large-scale surge level (i.e., at the scale of the southern North Sea, as imposed at the boundaries of the numerical model) to unravel its effect on the exchange flows. Locally generated gradients in surge levels in the tidal basin cause a water level difference between both sides of the tidal divides, which induces a residual flow between basins. These gradients are more significant than large-scale gradients in surge levels. Results of different model simulations show that the large-scale surge levels increase the magnitude of cumulative residual flows at tidal divides, due to larger flow depths and thus larger conveyance areas at the tidal divides. Large-scale surge levels thus facilitate locally generated residual flows rather than generate the residual flows itself, which implies nonlinear interactions between wind and surge.

Flow characteristics (e.g., velocity amplitude and phasing relative to water level variations) were found similar for measurement locations at each of the two tidal divides. The main reason why magnitudes of the residual discharges at the two tidal divides are different is therefore the difference in conveyance capacity, i.e., is largely attributed to the geomorphology of the basin. Different residual flows at the tidal divides are compensated by a residual flow through the tidal inlet. This is illustrated conceptually in Fig. 15. Wind from the prevailing wind direction at this site (i.e., west-southwest) causes a residual outflow through Ameland Inlet.

The exchange flows at the tidal divide of Terschelling in response to wind forcing have also been determined based on numerical modelling results by Duran-Matute et al. (2016). Characteristic values used to compare the results for different simulation periods are the residual flow during weak wind conditions (i.e., tide-averaged wind speed smaller than 2 m/s) and the wind-dependent variability. The latter is addressed using the wind direction dependent conductance of a wind-driven residual flow, which follows from a least squares fit between the residual

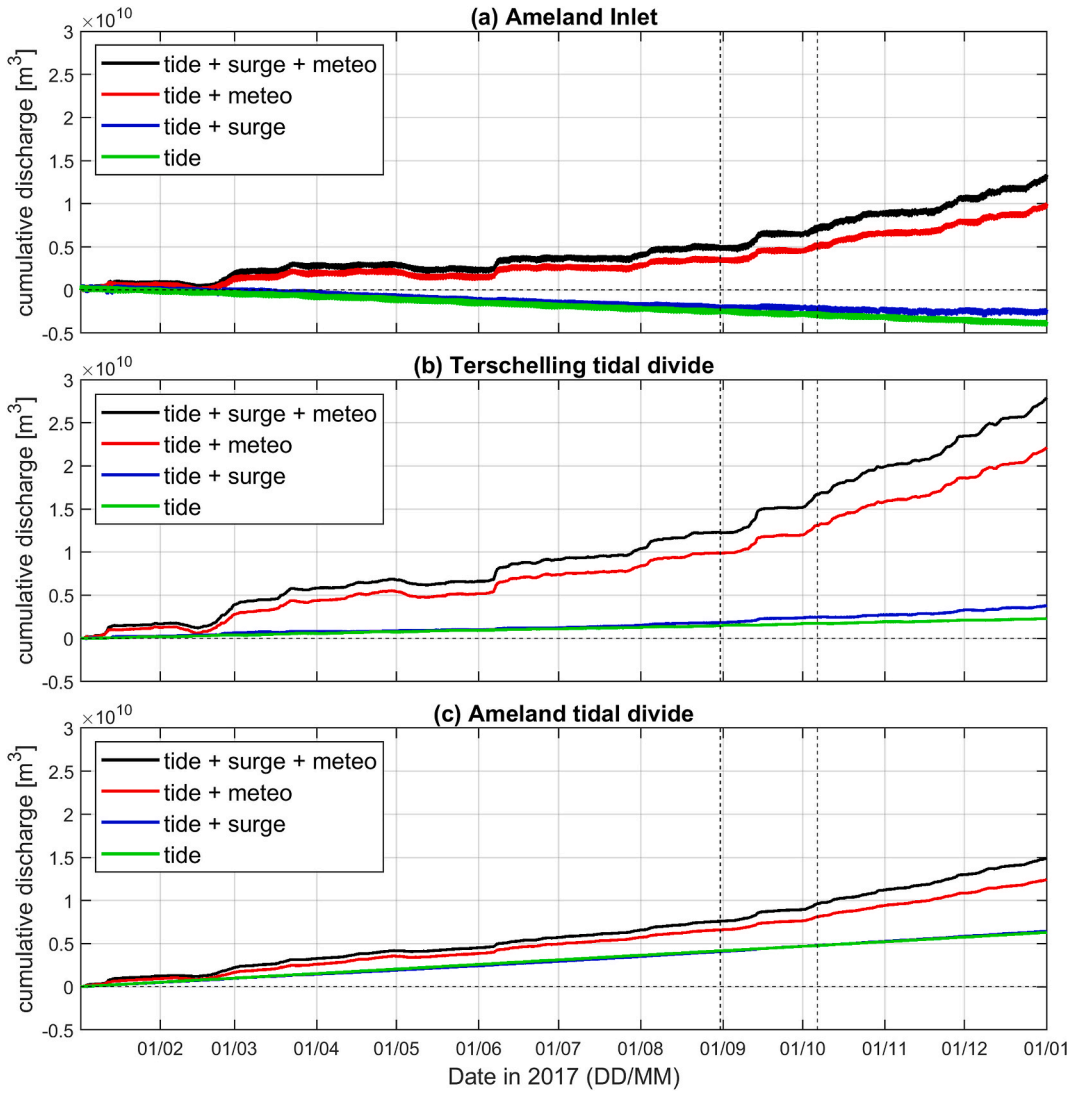

Fig. 13. Cumulative discharge in 2017 through [a] Ameland Inlet and over the tidal divides of [b] Terschelling and [c] Ameland in simulations with different forcing mechanisms. Outflow (i.e., ebb) through Ameland Inlet and eastward flow over the tidal divides are considered in positive direction. The vertical dashed lines indicate the duration of the field campaign.

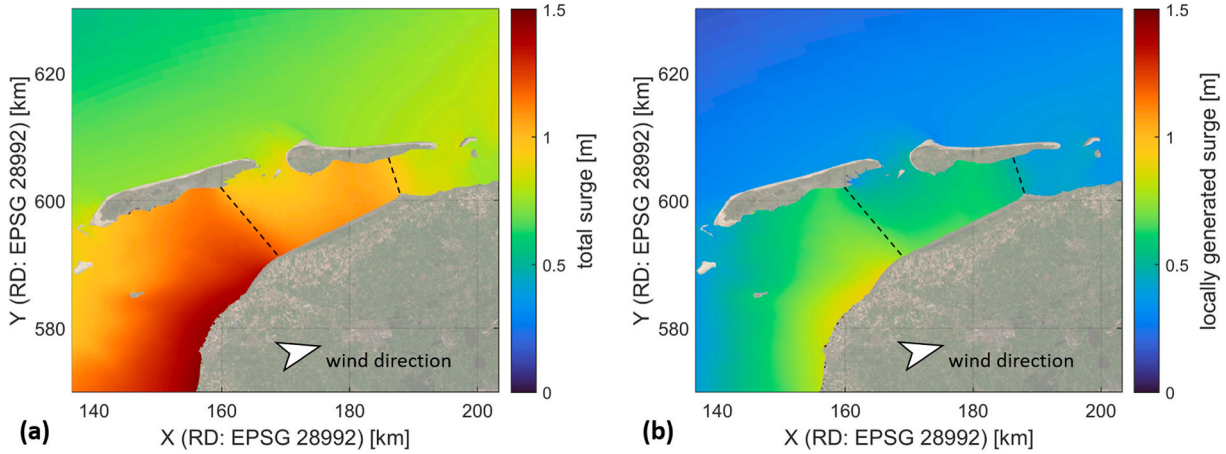

Fig. 14. Map of the [a] total surge and [b] locally generated surge at the moment of maximum residual flow over the two tidal divides in 2017 (i.e., September 13th, 13:00). Approximate locations of the tidal divides are indicated with dashed lines. Surge levels are determined relative to model results with only tidal forcing.

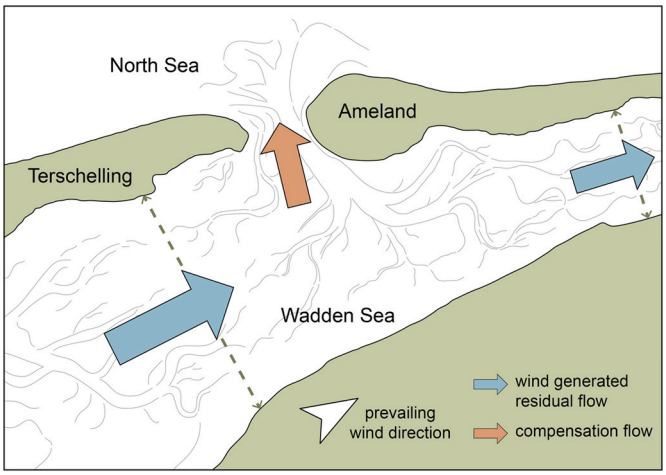

Fig. 15. Conceptual diagram of the residual exchange flows of the Ameland Inlet system during winds from the main westerly wind direction. Wind-generated residual flows at the two tidal divides are different in magnitude, leading to a residual outflow through Ameland Inlet.

discharge and the square of the wind speed (Duran-Matute et al., 2016). The residual discharge towards the east during weak wind conditions is similar but slightly larger compared to the previous study (57 m^3/s instead of 49 m^3/s). The preferential wind directions for throughflow over the watershed (west-southwest and north-northwest) and the conductance for wind from the preferential wind direction for westward flow (20 m/s) are the same. The conductance for wind from the preferential wind direction for eastward flow is with 41 m/s only slightly larger than 37 m/s in Duran-Matute et al. (2016). The similar model results indicate that the field observations at the tidal divides not only validate and support the model results in this study but also (the mechanisms behind) the results of Duran-Matute et al. (2016).

The wind-driven residual flows in Ameland Inlet system are in agreement with the general findings of Li (2013) in a schematized numerical modelling study of a multiple-inlet system. The prevailing wind direction being aligned with the back-barrier basin significantly influences the circulation flows between basins and leads to a residual outflow through the inlet in the downwind direction. Although it is not the most downwind inlet in the communicating multiple-inlet system, the funnelling shape of the basin still causes a residual outflow through Ameland Inlet. This system behaviour is very similar to the wind-driven circulation that is observed during strong south-westerly winds in the aligned basins of Borkum, Juist, Norderney and Baltrum in the East Frisian Wadden Sea, with inflow at the westernmost inlet, throughflow along the funnel-shaped basins and outflow at three inlets towards the east (Herrling and Winter 2015).

4.2. Representativeness of the measurement period

The exchange flows in the Ameland Inlet system were investigated using field observations with a duration of 36 days and using numerical modelling of one year (i.e., 2017). Two windstorms cause exchange flows across tidal divides during the field campaign to exceed yearly averaged conditions. The computed cumulative discharges during the field campaign through Ameland Inlet and over the tidal divides of Terschelling and Ameland are 17%, 16%, and 14% of the cumulative discharge in 2017, respectively. The measurements, however, only span 10% of the year. Although there were also periods in the field campaign with relatively small exchange flows (e.g., second half of September, see Fig. 13), the large residual flows during the two windstorms are dominant in contributing to total residual fluxes in the measurement period. Storm Sebastian on September 13 was responsible for the largest modelled residual flows in the whole year. The dataset with field observations thus captures a wide range of conditions, including conditions that show a lot of flow over the tidal divides, although it may not represent average conditions.

When compared to the average wind climate at Ameland, 2017 had slightly more westerly winds. Winds came from the western quadrant (225–315°N) during 42% of time in 2017 and during 34% of time in five years from 2013 to 2017. Since wind-generated flows at the tidal divides are relatively large during wind from the west, meteorological conditions in 2017 were thus favourable for large exchange flows between the tidal basins. Modelling this year helps to investigate the extent to which transport at the tidal divides leads to residual flows in the inlet, knowing that these are above average. The wind conditions in 2017 also explain why the cumulative discharge over the tidal divide of Terschelling ($2.8*10^{10}$ m^3; Fig. 13) is larger than in 2009–2011 (approximately $2.1*10^{10}$ m^3 per year), as determined by Duran-Matute et al. (2016).

4.3. Implications

It is supposed that the residual flows that are quantified in this paper will be reflected in net sediment transport rates and hence morphodynamic development. Although the quantitative effects are yet to be investigated by additional measurements and modelling, the hydrodynamic results may be used to formulate hypotheses. Since the availability of fine sediments is high near the tidal divides, energetic conditions (i.e., high waves) and large exchange flows are expected to transport large amounts of fine sediments to the neighbouring basin (e.g., Sassi et al. (2015)) and possibly also through the tidal inlet towards the ebb-tidal delta (Pearson et al., 2019). Frequent, high resolution bathymetric surveys of the Ameland ebb-tidal delta reveal that inlet-scale (O(10 km)) morphologic changes begin with small (O(100m)) shoal instabilities that expand rapidly (O(1yr)) (Elias et al., 2019). Large outflow events could be the trigger for the development of small shoals.

The variability in exchange flows between adjacent basins can also have important ecological consequences. Van der Veer et al. (1998) show that variability in hydrodynamic circulation patterns between years determines the fish larvae reaching the Wadden Sea from the spawning grounds. The study does not consider distribution of the larvae within the Wadden Sea, but it can be expected that similar mechanisms are present here. Mussel populations in neighbouring tidal basins of the Wadden Sea share temporal trends, although groups of tidal basins have independent time series (Folmer et al., 2014). Larval transport between adjacent basins by residual flows revealed in the present study may explain this synchrony. The improved insight into the exchange at tidal divides could be a basis for further unravelling such ecological relationships.

The results indicate that wind forcing causes most of the variability in exchange flows in the Ameland Inlet system. Wind events that occur relatively infrequently lead to exchange flows that are multiple times larger than during calm conditions. A magnitude-frequency analysis is needed to identify which conditions have most impact on the longer term (i.e., high-frequency low-energy events or low-frequency high-energy events).

5. Conclusions

Although Ameland Inlet system can be conceptually considered as a separate basin during calm conditions, wind-driven currents generated at tidal divides lead to significant residual flows between neighbouring basins. During wind from the prevailing wind direction (i.e., west-southwest), field measurements and numerical modelling indicate eastward wind-induced residual discharges over the tidal divides of Ameland Basin. During storms, the volume of water flowing per tidal period over Terschelling tidal divide into Ameland Basin can exceed the mean tidal prism of Ameland Inlet. High surge levels, induced by set up in the North Sea, increase the conveyance area at tidal divides and

facilitate exchange flows.

The magnitude of the residual discharges at each of the two tidal divide differs, primarily because of a difference in their conveyance capacity. The western tidal divide of the Ameland Basin has a larger conveyance capacity than the eastern tidal divide. This is compensated for by residual flows through Ameland Inlet, directed out of the tidal basin during wind from the prevailing southwestern wind direction. The residual outflow through the inlet is therefore a consequence of the wind-induced discharge over the tidal divides rather than the cause of the flow over the tidal divides. Given the variation in flow over the tidal divides with wind conditions, a seasonal variation in the residual exchange flows exists.

The orientation and geometry of shallow (intertidal) areas in relation to the wind climate in the basin is more significant for residual exchange flows in the Ameland Inlet system than the orientation of the main channels. We expect that these relations between system characteristics and the wind climate also hold elsewhere in the Wadden Sea and in other multiple tidal inlet systems, and therefore help to estimate and explain net inflow or outflow through tidal inlets.

Declaration of competing interest

The authors declare that they have no known competing financial interests or personal relationships that could have appeared to influence the work reported in this paper.

Acknowledgements

This work is part of the research programme 'Collaboration Program Water' with project number 14489 (SEAWAD), which is (partly) financed by NWO Domain Applied and Engineering Sciences. Special thanks to the Dutch Ministry of Infrastructure and Watermanagement (Rijkswaterstaat and Rijksrederij) for their ongoing support as part of the Kustgenese2.0 project. We gratefully acknowledge Peter Herman, Marion Tissier, and Floris de Wit for fruitful discussions and their input in this study. We are grateful to Ad van der Spek and two anonymous reviewers for their constructive feedback on this manuscript. Data from the 2017 Kustgenese2.0/SEAWAD field measurement campaing are available at the 4TU Centre for Research Data: https://doi.org/10.4121/collection:seawad.

References

Buijsman, M.C., Ridderinkhof, H., 2007. Long-term ferry-ADCP observations of tidal currents in the Marsdiep inlet. J. Sea Res. 57, 237–256.
Burchard, H., Flöser, G., Staneva, J.V., Badewien, T.H., Riethmüller, R., 2008. Impact of density gradients on net sediment transport into the Wadden Sea. J. Phys. Oceanogr. 38 (3), 566–587.
Charnock, H., 1955. Wind stress on a water surface. Q. J. Roy. Meteorol. Soc. 81 (350), 639–640.
Colosimo, I., de Vet, P.L.M., van Maren, D.S., Reniers, A.J.H.M., Winterwerp, J.C., van Prooijen, B.C., 2020. The impact of wind on flow and sediment transport over intertidal flats. J. Mar. Sci. Eng. 8 (11), 910.
Davis, R.A., Hayes, M.O., 1984. What is a wave-dominated coast? Mar. Geol. 60, 313–329.
Duran-Matute, M., Gerkema, T., 2015. Calculating residual flows through a multiple-inlet system: the conundrum of the tidal period. Ocean Dynam. 65 (11), 1461–1475.
Duran-Matute, M., Gerkema, T., De Boer, G.J., Nauw, J.J., Gräwe, U., 2014. Residual circulation and freshwater transport in the Dutch Wadden Sea: a numerical modelling study. Ocean Sci. 10 (4), 611–632.
Duran-Matute, M., Gerkema, T., Sassi, M.G., 2016. Quantifying the residual volume transport through a multiple- inlet system in response to wind forcing: the case of the western Dutch Wadden Sea. J. Geophys. Res.: Oceans 121 (12), 8888–8903.
Elgar, S., Raubenheimer, B., Guza, R.T., 2005. Quality control of acoustic Doppler velocimeter data in the surfzone. Meas. Sci. Technol. 16 (10), 1889–1893.
Elias, E.P.L., Cleveringa, J., Buijsman, M.C., Roelvink, J.A., Stive, M.J.F., 2006. Field and model data analysis of sand transport patterns in Texel Tidal inlet (The Netherlands). Coast Eng. 53 (5–6), 505–529.
Elias, E.P.L., Van der Spek, A.J.F., Pearson, S.G., Cleveringa, J., 2019. Understanding sediment bypassing processes through analysis of high-frequency observations of Ameland Inlet, The Netherlands. Mar. Geol. 415, 105956.
Elias, E.P.L., Van Der Spek, A.J.F., Wang, Z.B., De Ronde, J., 2012. Morphodynamic development and sediment budget of the Dutch Wadden Sea over the last century. Neth. J. Geosci. 91 (3), 293–310.
Folmer, E.O., Drent, J., Troost, K., Büttger, H., Dankers, N., Jansen, J., van Stralen, M., Millat, G., Herlyn, M., Philippart, C.J.M., 2014. Large-scale spatial dynamics of intertidal mussel (Mytilus edulis L.) bed coverage in the German and Dutch Wadden Sea. Ecosystems 17 (3), 550–566.
Goring, D.G., Nikora, V.I., 2002. Despiking acoustic Doppler velocimeter data. J. Hydraul. Eng. 128 (1), 117–126.
Herrling, G., Winter, C., 2015. Tidally- and wind-driven residual circulation at the multiple-inlet system East Frisian Wadden Sea. Continent. Shelf Res. 106, 45–59.
Hersbach, H., Bell, B., Berrisford, P., Hirahara, S., Horányi, A., Muñoz-Sabater, J., Nicolas, J., Peubey, C., Radu, R., Schepers, D., Simmons, A., Soci, C., Abdalla, S., Abellan, X., Balsamo, G., Bechtold, P., Biavati, G., Bidlot, J., Bonavita, M., Thépaut, J., 2020. The ERA5 global reanalysis. Q. J. Roy. Meteorol. Soc. 146 (730), 1999–2049.
Li, C., 2013. Subtidal water flux through a multiple-inlet system: observations before and during a cold front event and numerical experiments. J. Geophys. Res.: Oceans 118 (4), 1877–1892.
Liu, J.T., Aubrey, D.G., 1993. Tidal residual currents and sediment transport through multiple tidal inlets. Coast. Estuar. Stud. 44, 113–157.
Lodder, Q.J., Wang, Z.B., Elias, E.P.L., van der Spek, A.J.F., de Looff, H., Townend, I.H., 2019. Future response of the Wadden Sea tidal basins to relative sea-level rise - an aggregated modelling approach. Water 11 (10), 2198.
Maan, D.C., van Prooijen, B.C., Wang, Z.B., 2019. Progradation speed of tide-dominated tidal flats decreases stronger than linearly with decreasing sediment availability and linearly with sea level rise. Geophys. Res. Lett. 46, 262–271.
Mori, N., Suzuki, T., Kakuno, S., 2007. Noise of acoustic Doppler velocimeter data in bubbly flows. J. Eng. Mech. 133 (1), 122–125.
Nicholls, R.J., Cazenave, A., 2010. Sea-level rise and its impact on coastal zones. Science 328 (5985), 1517–1520.
Pearson, S., Van Prooijen, B., De Wit, F., Meijer-Holzhauer, H., De Looff, A., Wang, Z.B., 2019. Observations of suspended particle size distribution on an energetic ebb-tidal delta. Int. Conf. Coastal Sediments 2019, 1991–2003. https://doi.org/10.1142/9789811204487_0172.
Ridderinkhof, H., 1988a. Tidal and residual flows in the western Dutch Wadden Sea. I: numerical model results. Neth. J. Sea Res. 22 (1), 1–22.
Ridderinkhof, H., 1988b. Tidal and residual flows in the western Dutch Wadden Sea. II: an analytical model to study the constant flow between connected basins. Neth. J. Sea Res. 22, 185–198.
Sassi, M., Duran-Matute, M., van Kessel, T., Gerkema, T., 2015. Variability of residual fluxes of suspended sediment in a multiple tidal-inlet system: the Dutch Wadden Sea. Ocean Dynam. 65 (9–10), 1321–1333.
Van de Kreeke, J., Cotter, D.C., 1974. Tide-induced mass transport in lagoon-inlet systems. Coast Eng. 14, 2290–2301.
Van der Spek, A.J.F., 1995. Reconstruction of tidal inlet and channel dimensions in the Frisian Middelzee, a former tidal basin in the Dutch Wadden Sea. In: Tidal Signatures in Modern and Ancient Sediments. Special Publications International Association of Sedimentologists, pp. 239–258.
Van der Veer, H.W., Ruardij, P., Van den Berg, A.J., Ridderinkhof, H., 1998. Impact of interannual variability in hydrodynamic circulation on egg and larval transport of plaice Pleuronectes platessa L. in the southern North Sea. J. Sea Res. 39 (1), 29–40.
Van der Werf, J., Antonio Álvarez Antolïnez, J., Brakenhoff, L., Gawehn, M., Den Heijer, K., De Looff, H., Van Maarsseveen, M., Holzhauer, H., Mol, J.-W., Pearson, S., Van Prooijen, B., Santinelli, G., Schipper, C., Tissier, M., Tonnon, P.K., De Vet, L., Vermaas, T., Wilmink, R., De Wit, F., 2019. Datareport Kustgenese 2.0. *Deltares Report 220339-015-ZKS-0004* (The Netherlands).
Van Goor, M.A., Zitman, T.J., Wang, Z.B., Stive, M.J.F., 2003. Impact of sea-level rise on the morphological equilibrium state of tidal inlets. Mar. Geol. 202, 211–227, 2003.
Van Prooijen, B.C., Wang, Z.B., 2013. A 1D model for tides waves and fine sediment in short tidal basins - application to the Wadden Sea. Ocean Dynam. 63, 1233–1248.
Van Prooijen, B., Tissier, M., de Wit, F., Pearson, S., Brakenhoff, L., van Maarseveen, M., van der Vegt, M., Mol, J.-W., Kok, F., Holzhauer, H., van der Werf, J., Vermaas, T., Gawehn, M., Grasmeijer, B., Elias, E., Tonnon, P.K., Reniers, A., Wang, Z.B., den Heijer, C., de Looff, H., 2020. Measurements of hydrodynamics, sediment, morphology and benthos on Ameland ebb-tidal delta and Lower shoreface. Earth Syst. Sci. Data 12, 2775–2786.
Vinther, N., Christiansen, C., Bartholdy, J., Sorensen, C., Lund-Hansen, L.C., 2004. Sediment transport across a tidal divide in the Danish Wadden Sea. Geografisk Tidsskrift - Danish Journal of Geography 104, 71–86.
Wang, Z.B., Elias, E.P.L., Van der Spek, A.J.F., Lodder, Q.J., 2018. Sediment budget and morphological development of the Dutch Wadden Sea: impact of accelerated sea-level rise and subsidence until 2100. Neth. J. Geosci. 97 (3), 183–214.
Wang, Z.B., Vroom, J., Van Prooijen, B.C., Labeur, R.J., Stive, M.J.F., 2013. Movement of tidal watersheds in the Wadden Sea and its consequences ont he morphological development. Int. J. Sediment Res. 28 (2), 162–171.
Zijl, F., Verlaan, M., Gerritsen, H., 2013. Improved water-level forecasting for the Northwest European Shelf and North Sea through direct modelling of tide, surge and non-linear interaction. Ocean Dynam. 63 (7), 823–847.